JOURNAL OF GEOPHYSICAL RESEARCH, VOL. 103, NO. C12, PAGES 27,999–28,012, NOVEMBER 15, 1998

The development and operational application of nonlinear algorithms for the measurement of sea surface temperatures with the NOAA polar-orbiting environmental satellites

C. C. Walton, W. G. Pichel, and J. F. Sapper

NOAA, National Environmental Satellite, Data, and Information Service, Washington, D. C.

D. A. May

Naval Oceanographic Office, Department of the Navy, Stennis Space Center, Mississippi

Abstract. Since 1990, the NOAA National Environmental Satellite Data and Information Service (NESDIS) has provided satellite-derived sea surface temperature (SST) measurements based on nonlinear SST algorithms, using advanced very high resolution radiometer (AVHRR) multiple-infrared window channel data. This paper develops linear and nonlinear SST algorithms from the radiative transfer equation. It is shown that the nonlinear algorithms are more accurate than linear algorithms but that the functional dependence of the nonlinearity is data dependent. This theoretical discussion (sections 2–4) is followed with a discussion in section 5 of the accuracy over a 9-year period of the satellite-derived SST measurements provided by NOAA NESDIS when compared with coincident drifting buoys. Between 1989 and 1998 the global scatter of the daytime satellite SST against drifting buoy measurements has decreased from ~0.8° to 0.5°C, while the nighttime scatter has remained fairly constant at 0.5°C. An exception to these accuracy measurements occurred after the eruption of Mount Pinatubo in June 1991.

1. Introduction

Sea surface temperature (SST) measurements currently have a wide variety of applications, some of which have stringent accuracy requirements. Typical applications include (1) input to numerical ocean and atmospheric models [*Reynolds and Marsico*, 1993; *Schwab and Bedford*, 1994], (2) tactical support to oceanographic surveys and interpretation of surface oceanographic features in support of fisheries science or physical oceanographic research [*Simpson*, 1994; *Laurs and Brucks*, 1985], (3) tactical support of commercial fishing activities [*Myers and Hick*, 1990], (4) protection of endangered species such as sea turtles [*Epperly et al.*, 1995], (5) study of red tide outbreaks [*Chester and Wolf*, 1990], (6) derivation of ocean feature charts and ocean surface current measurements useful in support of ship routing and search and rescue activities [*Breaker et al.*, 1994], (7) analysis of short- and long-term fluctuations in ocean temperature and associated atmospheric effects, such as El Niño/Southern Oscillation [*Ji et al.*, 1995; *Strong*, 1986], (8) climate change studies [*Reynolds et al.*, 1989], and (9) monitoring coral reef bleaching [*Strong et al.*, 1997].

Numerous surveys and workshops have been conducted over the years to obtain accuracy and other requirements for satellite-derived products, including SST [*Sherman et al.*, 1980; *Hussey*, 1985; *Cornillon*, 1989]. These requirements for the civilian community have been consolidated with those from the Department of Defense to form the SST requirements currently being considered for the convergence of the military and civilian polar satellite systems into the National Polar-Orbiting Operational Environmental Satellite System (NPOESS). The current NPOESS requirement for SST accuracy is ±0.5°C as a "threshold" or minimum requirement and ±0.1°C as an "objective" or desirable goal. The more stringent accuracy is required for climate applications with spatial and temporal averaging permitted (i.e., 50–250 km spatial resolution averaged for 0.5–3 months). In general, climate applications require accuracies in the 0.1°–0.3°C range [*Yates et al.*, 1985; *Cornillon*, 1989; *Jacobowitz*, 1997], whereas numerical weather prediction, fisheries, coastal management, and most other applications of satellite SST data require accuracies around 0.5°C for individual measurements at high spatial resolution (0.5–10 km) and with revisit times of two to four observations per day [*Hussey*, 1985].

The advanced very high resolution radiometer (AVHRR/2) instrument, first flown on the NOAA 7 satellite in 1981, was designed primarily for cloud imaging and measurement of SST. It includes five channels, channel 1 in the visible spectral range (0.58–0.68 μm), channel 2 in the near-infrared reflective region (0.72–1.18 μm), and three channels in the thermal infrared emission "window" spectral region: channel 3 (3.55–3.95 μm), channel 4 (10.3–11.3 μm), and channel 5 (11.5–12.5 μm). The last three channels are called window channels because radiation from Earth's surface in these spectral regions is only weakly attenuated by the atmospheric constituents; these channels are therefore useful for measuring SST. The potential for achieving the accuracy requirements of SST with AVHRR data, as described previously, arrives from several sources, as follows.

1. The multiple window channels provide a means for both correcting atmospheric attenuation and detecting cloud contamination in a single channel measurement.
2. The visible and reflective IR channels provide a cloud detection capability during the day.

Paper number 98JC02370.

3. The high resolution of the global coverage data (4 km) allows for measurements of dynamic ocean thermal structure and allows for measurements between cloud elements.

4. The low noise levels of the instrument output signal, expressed as a noise equivalent temperature difference ($NE\Delta T < 0.1°C$) in the window channels, and the high resolution of the AVHRR channel data determine the accuracy of the atmospheric correction algorithms and allow for uniformity cloud tests, which are extremely sensitive to partial cloudy conditions.

5. The instrument data together with ground-based processing provide an in-flight nonlinear calibration in the thermal channels, which removes detector or instrument drift and provides a correction for detector nonlinearities and other calibration inconsistencies [*Walton et al.*, 1998].

The potential for highly accurate measurements of SST with the AVHRR instrument has led to considerable interest within the research community in the assessment and development of new multiple-channel sea surface temperature (MCSST) algorithms since the launch of NOAA 7. Recent examples include those developed by *Walton* [1988], *Barton et al.* [1989], *Minnett*, [1990], *Bates and Diaz* [1991], *Yokoyama and Tanba* [1991], *Sakaida and Kawamura* [1992], *Harris and Mason* [1992], *Emery et al.* [1994], *Sobrino et al.* [1994], and *Yu and Barton* [1994]. *Barton* [1995] provides an interesting comparison between these examples and other SST algorithms. These algorithms make use of the fact that the attenuation by water vapor is different in each window channel, so that the total attenuation in one channel can be estimated from the measured temperature difference between any two channels. The theoretical development is based on the so-called split-window algorithm using channels 4 and 5 in the 11–12 μm region [*McMillin and Crosby*, 1984], but the results are applied to other channel combinations as well, e.g., the dual-window algorithm using channels 3 and 4, and the triple window algorithm, which employs channels 3, 4, and 5.

Since 1981, the National Oceanic and Atmospheric Administration (NOAA) National Environmental Satellite, Data and Information Service (NESDIS) has continuously been providing measurements of SST at an 8 km resolution over the globe using satellite data from the five-channel AVHRR/2 on the Polar-Orbiting Operational Environmental Satellites (POES). Through 1997, instruments from five different spacecraft have been utilized for this purpose (NOAA 7, 9, 11, 12, 14). *McClain et al.* [1985] describe the initial global processing procedures which were developed at NESDIS both for cloud detection and for estimating SST using linear algorithms based on the multiple-channel AVHRR data. This paper describes refinements to the SST algorithms, in particular, the development of nonlinear algorithms for estimating SST, which have improved the accuracy of the SST product. It must be stressed that cloud detection is critical to achieving accurate SST measurements and refinements have also been made to the NESDIS cloud detection procedures since 1985. These refinements include the use of high-resolution infrared sounder (HIRS/2) data, coincident with the AVHRR data, which is helpful for detecting certain uniform cloud situations at night [*Walton*, 1987] and for providing satellite SST coverage in Sun glitter regions during the daytime. These cloud detection improvements have also been implemented at the Naval Oceanographic Office and are described by *Kidwell* [1995] and *May et al.* [1998]. In general, the basic philosophy for data processing at NESDIS has not changed since 1985, namely, the use of global rather than regional algorithms both for cloud detection and computing SST. This avoids the problem of possible discontinuities at regional boundaries as well as any need for seasonal adjustments within regions.

The following three sections describe the theoretical development and application of the nonlinear SST algorithms used for operational SST calculation from AVHRR data. This theoretical development is followed by a concluding section describing the performance of the operational algorithms over time.

2. Development of Nonlinear SST Algorithms

McClain et al. [1985] describe the development of linear MCSST algorithms for estimating SST with the AVHRR window channel data. These algorithms assume that the temperature depression of one window channel measurement from the actual ocean surface temperature, $T_s - T_i$, is linearly proportional to the temperature difference of two window channel measurements, $T_i - T_j$. *Walton* [1988] describes a further development of this technique which results in a nonlinear proportionality between these parameters, an algorithm which has been designated the cross-product sea surface temperature algorithm (CPSST). Subsequent refinements to the CPSST algorithm resulted in implementation of this algorithm for global processing of SST with AVHRR data beginning in March 1990. An additional simplification of the CPSST, designated the nonlinear SST algorithm (NLSST), has been operational at NESDIS since April 1991. We will first derive these new algorithms from first principles, starting with the radiative transfer equation, and subsequently, compare these three algorithms for accuracy both in simulation and in the actual open ocean using drifting buoy measurements for ground truth.

The reason that the AVHRR window channels are useful for measuring SST can be understood in terms of the radiative transfer equation, which states that in a uniform scene, the measured radiance at the satellite I at wavenumber ν is composed of a surface contribution and an atmospheric contribution:

$$I(\nu) = B(\nu, T_s)\tau + \int_{\tau}^{1} B(\nu, T_P)\, d\tau \qquad (1)$$

This simplified form of the radiative transfer equation is applicable in the 11–12 μm spectral region because the sky and solar radiation reflected by Earth and clouds is negligible compared to the infrared emission, and Earth's ocean surface is very nearly a blackbody [*Smith et al.*, 1974]. This equation states that the net radiation at wavenumber ν measured at the top of the atmosphere consists of a surface emitted Planck radiance, $B(\nu, T_s)$, which is partially absorbed by the atmosphere, plus a summation of the net emission minus absorption of radiance by each layer of the atmosphere. This summation is a function of the concentration of the atmospheric constituents as well as the temperature at each pressure level in the atmosphere, T_p. With the mean value theorem of calculus, this equation can be simplified to

$$I(\nu) = B(\nu, T_s)\tau + \mathbf{B}(\nu)(1 - \tau) \qquad (2)$$

In these equations, T_s represents the temperature of the surface, whether it be the sea surface or an opaque, nontransmissive cloud top; τ is the transmittance from the surface to the top of the atmosphere; $\mathbf{B}(\nu)$ is a mean atmospheric Planck radiance computed from the second term in (1).

Because the transmission of the atmosphere in the AVHRR window channels is near unity, the radiative transfer equation (2) can be converted from radiance units to temperature units by expanding the Planck function B about the surface temperature T_s using a Taylor series to yield

$$T(\nu) = T_s + [\mathbf{T}(\nu) - T_s](1 - \tau) \tag{3}$$

where $T(\nu)$ is the brightness temperature that would be measured at the top of the atmosphere and $\mathbf{T}(\nu)$ is a weighted mean atmospheric temperature corresponding to $\mathbf{B}(\nu)$ in (2). In the 11–12 μm spectral region, corresponding to channels 4 and 5 of the AVHRR, the primary atmospheric absorber is water vapor, and (3) may be expressed in terms of the water vapor absorption coefficient associated with each channel, k_i and k_j, and the total water vapor path length w, where $\tau_i \approx 1 - k_i w$,

$$\begin{aligned} T_i &= T_s - k_i b_i \\ T_j &= T_s - k_j b_j \end{aligned} \tag{4}$$

and $b_i = w[T_s - \mathbf{T}_i]$. Equation (4) applies to one satellite measurement made in two window channels of the AVHRR, and in general, the parameter w will vary with each measurement. The MCSST solution is obtained from this set of linear equations under the assumptions that k_i and k_j are known constants (or have a constant ratio) and that the channel atmospheric temperatures are equal, $\mathbf{T}_i = \mathbf{T}_j$, or alternatively, $b_i = b_j$, yielding the following solution for T_s:

$$\mathrm{MCSST}(i, j) = T_i + \Gamma(T_i - T_j) \tag{5}$$

where $\Gamma = k_i/(k_j - k_i)$. This MCSST algorithm was first suggested by *Prabhakara et al.* [1974] and *McMillin* [1975]. An alternative procedure, which involves less restrictive assumptions, is to collect an ensemble of satellite measurements and to sort the data into bins of constant channel temperature measurements, T_i and T_j. Within each bin, we assume that the absorption coefficient is constant. Summing (4) over a collection of n measurements within one bin, we obtain

$$\begin{aligned} nT_i &= \sum T_s - k_i \cdot \sum b_i \\ T_i &= \mathrm{SST}_i - k_i \bar{b}_i \end{aligned} \tag{6}$$

where SST_i and $\bar{b}_i$ are simply the mean values within the summations indicated above. These quantities are functions of the channel measurement T_i because the summations are channel dependent. The parameter SST_i can be interpreted as a single channel temperature estimate of the actual surface temperature T_s. Equation (6) defines the absorption coefficient as a function of the channel temperature measurement T_i:

$$k_i = (\mathrm{SST}_i - T_i)/\bar{b}_i(T_i) \tag{7}$$

A theoretical discussion of the temperature dependence of the water vapor absorption coefficients in the 11–12 μm spectral region is given by *Prabhakara et al.* [1974]. Substituting (7) into (4) yields

$$\begin{aligned} T_i &= T_s - (\mathrm{SST}_i - T_i) b_i/\bar{b}_i(T_i) \\ T_j &= T_s - (\mathrm{SST}_j - T_j) b_j/\bar{b}_j(T_j) \end{aligned} \tag{8}$$

Making the assumption that $b_i/\bar{b}_i(T_i)$ equals $b_j/\bar{b}_j(T_j)$ and solving the set of linear equations (8), one obtains the following solution for T_s, which is designated the CPSST solution:

$$\mathrm{CPSST}(i, j) = T_i + \frac{\mathrm{SST}_i - T_i}{\mathrm{SST}_j - T_j + T_i - \mathrm{SST}_i}(T_i - T_j) \tag{9}$$

It should be noted that this nonlinear CPSST solution involves much less restrictive assumptions than does the MCSST solution. The absorption coefficients k_i are no longer restrained to be universal constants, and the effective mean atmospheric temperature $\mathbf{T}_i$ need not be the same in the two split-window channels. The restrictive assumptions associated with the MCSST solution can result in significant errors (of several degrees in some cases) in the retrieved SST [*Hagan*, 1989]. Equation (9) has an interesting interpretation. When the two single-channel solutions (SST_i, SST_j) are equal, they are the best estimate of the surface temperature, and the CPSST becomes identical to them. This condition only occurs in a typical or climatological atmosphere. In an atypical atmosphere the two single-channel solutions diverge, and the multichannel CPSST solution yields the greatest accuracy.

The single-channel solutions, SST_i, must be specified before (9) can be applied. Although other forms have been considered, a simple linear expression of the form,

$$\mathrm{SST}_i = AT_i + B \tag{10}$$

where A and B are channel dependent and are derived by simple linear regression against a data set of coincident buoy and satellite temperature measurements, is quite satisfactory. Additional details, such as a graphical interpretation of the solutions defined with (5) and (9), and the application of (9) to the nighttime dual-window or triple-window combinations of window channels, which requires the introduction of an additional adjustable parameter, are not germane to the derivation of the new NLSST formalism but are discussed by *Walton* [1988].

It is seen that (9) is of the same form as (5) but that the gamma parameter Γ has a specific two-channel temperature dependence. We shall investigate this dependence using a simulation data set and a data set composed of NOAA 14 measurements over the open ocean, coincident with drifting buoy measurements. A simulation of the influence of an aerosol-free atmosphere upon measurements in the three AVHRR window channels is performed using a procedure developed at NESDIS [*Weinreb and Hill*, 1980]. The model calculations include the effects of water vapor, molecular nitrogen, and the uniformly mixed gases CO_2, N_2O, CO, and CH_4. Specifically excluded are ozone, aerosols, and water clouds. Also, nonzero surface reflectivity effects are not included. More sophisticated radiative transfer models may be available, but what distinguishes this model is the ease with which it is applied to a diverse set of 115 marine atmospheric profiles to determine cloud-free simulated channel temperature measurements in each of the three AVHRR/2 window channels. The set of marine profiles covers the entire range of SSTs and moisture conditions ranging from 0.5 to 5.5 cm of precipitable water. With this simulated data set, the gamma parameter Γ is plotted as a function of the surface temperature and the channel temperature difference, $T_4 - T_5$, in Figures 1–3. The plots in Figures 1 and 2 are derived from the simulation multichannel data set. However, the single-channel solutions (10), which define gamma with (9), are computed two different ways. A linear regression against the simulated channel temperature measurements using radiosonde measurements of surface air temperature as ground truth defines the "simulation gamma"

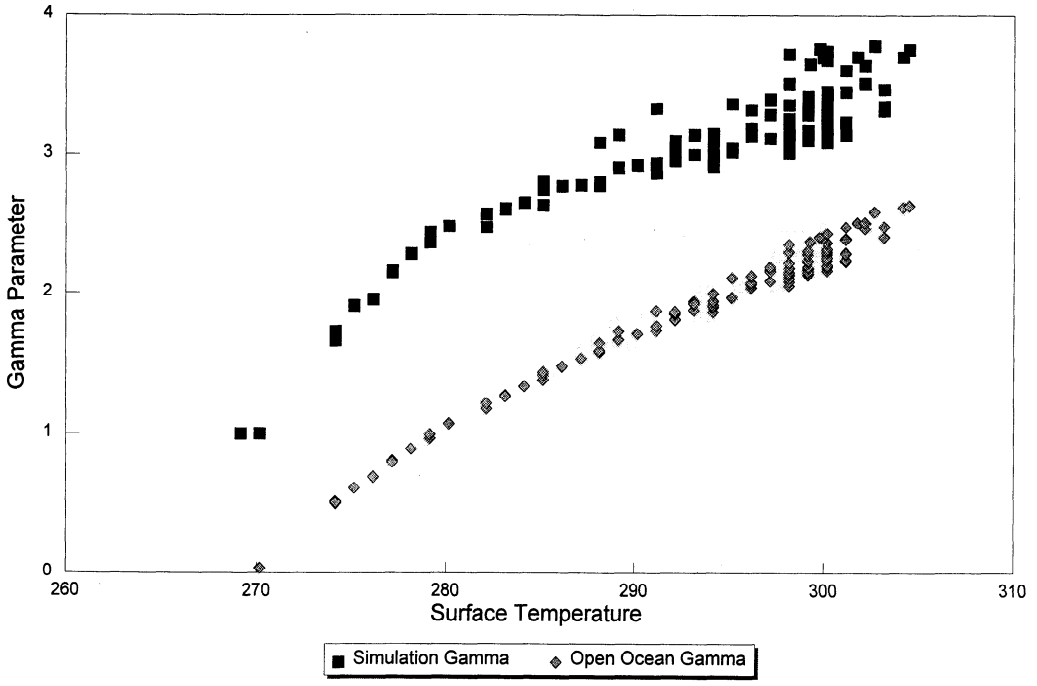

Figure 1. The CPSST split-window gamma parameter plotted with simulation data as a function of the radiosonde air surface temperature. The gamma parameter is computed twice, once using the single channel solutions, SST_i, obtained from the simulation data and a second time using the single channel solutions obtained with open ocean AVHRR data. A value of 1 has been added to the gamma parameter in the top plot to separate the data.

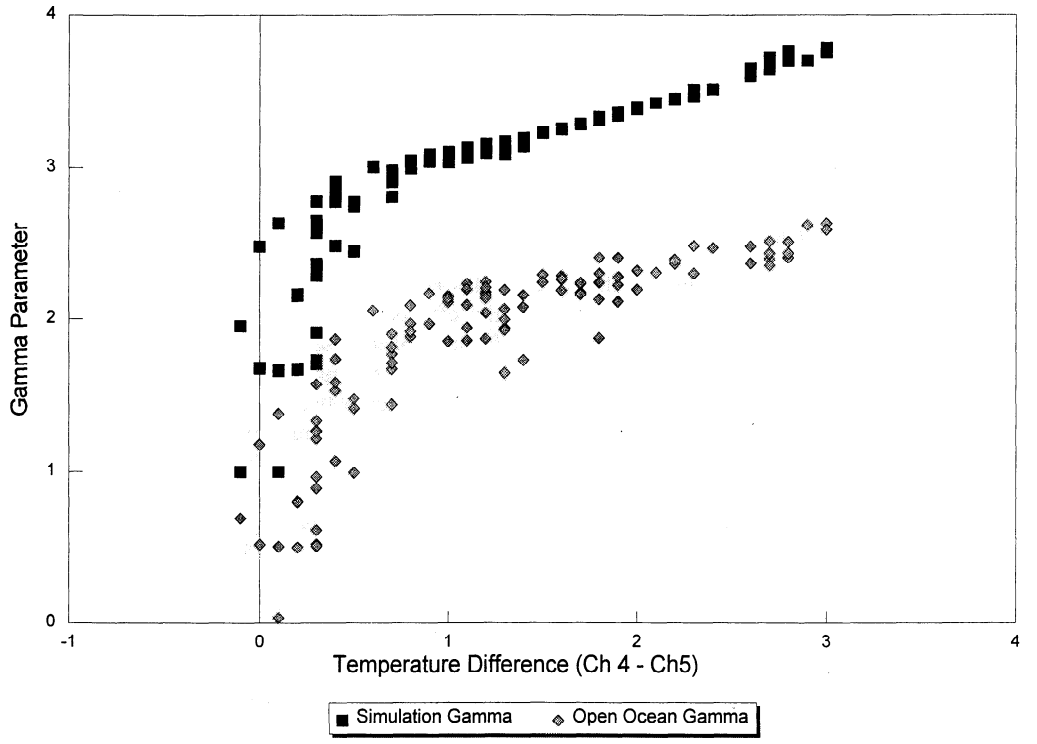

Figure 2. The CPSST split-window gamma parameter plotted with simulation data as a function of the simulated AVHRR channel temperature difference (channel 4 − channel 5). The gamma parameter is computed twice, once using the single channel solutions, SST_i, obtained from the simulation data and a second time using the single channel solutions obtained with open ocean AVHRR data. A value of 1 has been added to the gamma parameter in the top plot to separate the data.

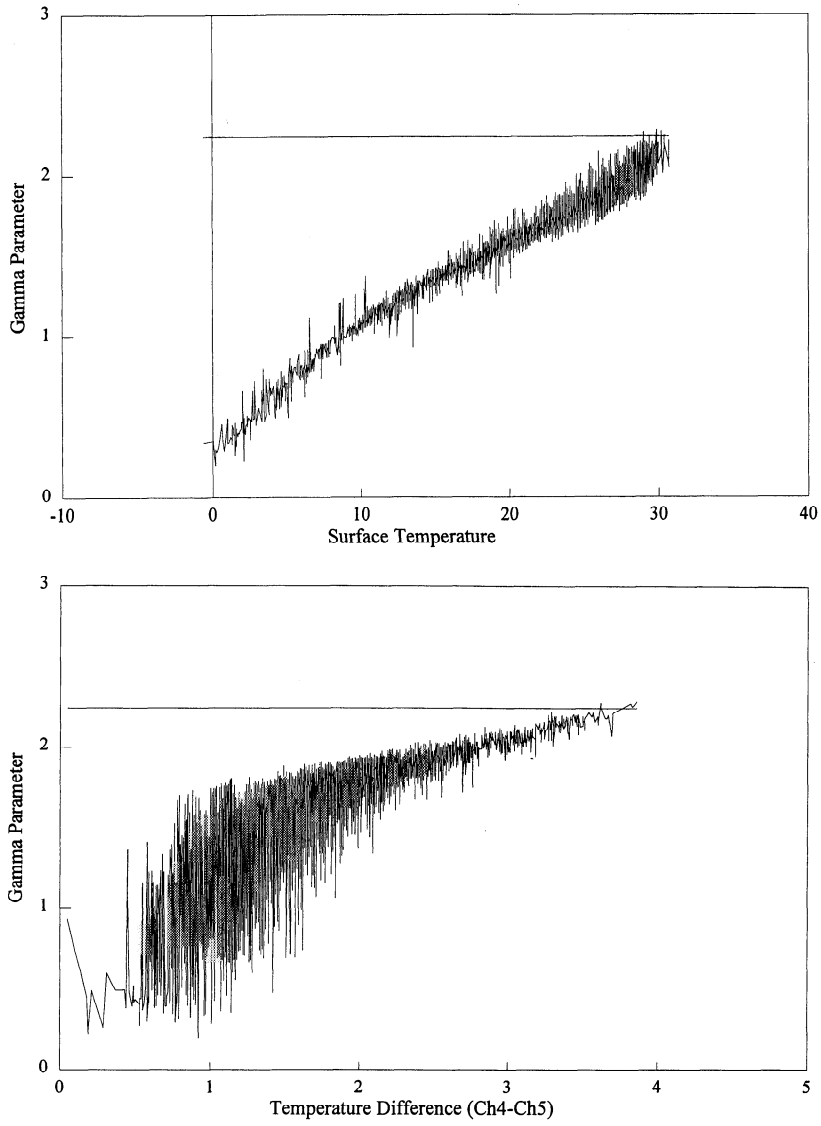

Figure 3. The CPSST split-window gamma parameter plotted with January 1996 open ocean data as a function of both the NESDIS 100 km analysis estimate of surface temperature and the open ocean AVHRR channel temperature difference (channel 4 − channel 5). The gamma parameter is computed using the single channel solutions obtained with open ocean AVHRR data. Each plot is composed of over 4000 data points. The horizontal bar represents the value of the MCSST gamma parameter.

values, while a linear regression against open ocean channel temperature measurements using coincident drifting buoy temperature measurements as the dependent parameter defines the "open ocean gamma" values. As a comparison, Figure 3 plots the open ocean gamma parameter using open ocean data obtained from NOAA 14.

An examination of Figures 1 and 2 shows a striking difference in the functional dependence of the two gamma parameters. The simulation gamma parameter is highly correlated to the channel temperature difference, $T_4 - T_5$, in all but very dry atmospheres. The statistical least squares regression correlation R^2 is 0.95 for channel temperature differences above 0.5°C, while the correlation with surface temperature is weaker ($R^2 = 0.58$) for the same data. This implies that the correction algorithm for atmospheric absorption can be expressed as a simple quadratic function of this temperature difference. This form of solution has been considered in previous theoretical studies [*McMillin*, 1975; *Emery et al.*, 1994]. On the other hand, Figures 1 and 2 indicate that the open ocean gamma parameter is better correlated to the ocean surface temperature ($R^2 = 0.92$) than it is to the channel temperature difference ($R^2 = 0.66$). Figure 3 demonstrates that the previous statement applies when the open ocean gamma parameter is plotted using open ocean data. This discrepancy between the results obtained with the simulation gamma and the open ocean gamma may result from various error sources in the data used to define gamma. The simulation data contain no error other than that inherent in approximating the transmittances of the various atmospheric constituents. In the 11–12 μm spectral range these errors are thought to be quite small, less than 0.3°C absolute temperature error [*Weinreb and Hill*, 1980]. Since the simulated temperature errors would be highly correlated in these two channels, the error in the channel difference, $T_4 - T_5$, should be considerably less than 0.3°C. The open ocean satellite measurements include many error sources or discrepancies not modeled by the simulation data

Table 1. NLSST Accuracies Using Various Estimates of Surface Temperature (T_{sfc}): September 1992 Daytime Buoy Matchups

	T_{sfc}		
	Satellite 100 km Analysis	1° Robinson Climatology	MCSST Algorithm
T_{sfc} Accuracy (T_{sfc} − buoy), °C			
Scatter	0.63	0.83	0.66
Bias	−0.1	−0.22	0.07
NLSST Accuracy (T_{sfc} − buoy), °C			
Scatter	0.61	0.58	0.66
Bias	0.05	0.02	0.07
CORR (NLSST − buoy, T_{sfc} − buoy) correlation	0.46	0.15	0.91

N = 1108. Bias is the mean difference between satellite SST and buoy SST (satellite − buoy); scatter is the standard deviation of the satellite − buoy differences.

set. These include among others, instrumental noise, residual cloud contamination, solar heating on a calm ocean surface, residual calibration errors, etc. The SST algorithms magnify these errors, some more than others. For instance, high very thin cirrus clouds are pervasive and depress the individual channel measurements only slightly but can increase the channel 4 minus 5 temperature difference significantly [*Prabhakara et al.*, 1988]. Also, solar heating of the ocean surface tends to increase the channel 4 minus 5 difference, especially in a moist atmosphere, since surface-emitted radiance in the channel 4 spectral range is absorbed less by the atmospheric water vapor than is radiance emitted in the channel 5 spectral range. Consequently, the channel 4 measured temperature responds greater to a change in surface temperature while the atmosphere remains constant than does the channel 5 measurement. Anomalous large channel temperature differences would have a much larger impact on a correction algorithm which is a quadratic function of the difference than one that is a linear function of this difference. Additionally, the open ocean data plotted in Figure 3 are obtained at different viewing angles ranging up to 53° satellite zenith angle, while the simulation data plotted in Figures 1 and 2 assume a nadir viewing angle. Further, the measured data include discrepancies between the ocean skin temperature measured by the satellite and the underlying mixed layer or bulk temperature measured by the drifting buoys. These discrepancies can result from solar heating or evaporative cooling of the skin or large discontinuities between the air surface and bulk ocean temperatures. These discontinuities are not included in the simulation data. Thus the differences shown in Figures 1 and 2 reflect a capability of the CPSST formulation to provide a gamma parameter which yields an optimal but different solution with these two very different data sets.

3. The NLSST Formalism

With actual open ocean satellite measurements, Figures 1–3 suggest that the gamma parameter of the CPSST solution can be approximated with a linear function of the surface temperature. The NLSST algorithm assumes this functional relationship

$$\mathrm{NLSST}(i, j) = T_i + \Gamma(T)[T_i - T_j] \qquad (11)$$

where the gamma parameter Γ equals a constant times an external estimate of the ocean surface temperature in units of °C.

One advantage of this approximation is that it removes or greatly reduces any dependence of the gamma parameter upon the satellite measurements. It has been demonstrated that a typical AVHRR channel 4 and 5 sensor noise value of 0.05°C results in a 0.33°C error in the output temperature from the CPSST algorithm, due partly to the fact that the input error propagates into the gamma parameter [*May*, 1993]. As a comparison, the same noise fed into the MCSST or the NLSST algorithms results in an output temperature error of 0.20°C. The disadvantage of the NLSST approximation is that the surface temperature is not known a priori and must be approximated. One must consider what accuracy and resolution are required for this estimate in order to accurately measure dynamic temperature structures in the ocean. A discussion of (11) is useful in this regard.

The first term is a single-channel measurement which includes the thermal structure of the ocean surface. The second term, which is a function of the temperature difference in two window channels, provides a measure of the effect of atmospheric absorption of the single-channel surface radiance measurement that results from absorption and reemission by the overlying atmosphere, primarily by water vapor. Figures 1 and 3 suggest that this second term should also be a function of the underlying surface temperature, which provides a measure of the allowable range of precipitable water vapor in the lower atmosphere. Because this second term is describing the effect of the atmosphere, which does not possess the horizontal temperature structure present in the ocean skin, it is not obvious that a high-resolution dynamical estimate of surface temperature is necessary or desirable in this application. Rather, a lower resolution climatological temperature estimate may be more useful.

A comparison of the effect of applying different estimates of surface temperature in the NLSST algorithm is provided in Table 1. This table includes satellite measurements collected over the entire globe in 1 month and matched within 4 hours and 25 km with drifting buoy measurements. Three different estimates of surface temperature, which define the gamma parameter, are considered. One estimate is an analysis produced by NESDIS from previous orbits of AVHRR SST data. This analysis is maintained on a 1° latitude/longitude grid mesh with a resolution of approximately 100 km for both northern and southern hemispheres. Further details concerning the production of this analysis are given by *McClain et al.* [1985]. A second low-resolution estimate is derived from a monthly cli-

matological temperature analysis on a 1° latitude/longitude square grid mesh [*Robinson*, 1976]. The third estimate is the MCSST algorithm value, which is then applied to (11). This MCSST estimate is obtained from the same satellite measurements and is at the same resolution as the NLSST value, namely, 8 km. The first row in the table shows the scatter and bias of each of the three temperature estimates T_{sfc} relative to the buoy temperature measurements. The second row gives the scatter and bias of the NLSST values corresponding to the three estimates of gamma derived from T_{sfc}. The surprising result is that the Robinson climatology, which has the greatest scatter (0.83°C) against the drifting buoy measurements, produces the most accurate NLSST algorithm. This result demonstrates the sensitivity of the NLSST algorithm to any correlation between the errors in the gamma parameter and errors in the satellite measurements. This correlation is computed using standard statistical procedures and provided in the third row of the table. The result also demonstrates the relative insensitivity of the NLSST to errors in the climatological temperature.

With the NLSST equations listed in Table 2, it is apparent that the NLSST error resulting from a 1°C error in T_{SFC} is a function of the $T_4 - T_5$ temperature difference. The worst case would occur in the tropics, where a typical $T_4 - T_5$ value might be 3°C. In this case a 1° error in T_{SFC} would produce approximately a 0.25°C error in the NLSST. Perhaps fortuitously, a low-resolution dynamic climatology should not yield errors much greater than 1° in the tropics, since there is little ocean temperature structure there. However, because of its low resolution, the Robinson climatology should not be used near coastlines and will not reflect anomalous climatological conditions such as El Niño; thus the NESDIS analysis is used operationally to compute the global NLSST measurements. Other ocean temperature analyses could be applied in this connection, such as the optimum interpolation analysis developed at the National Centers for Environmental Prediction (NCEP) which is being used in the NLSST algorithms being produced for the NOAA/NASA Ocean Pathfinder reprocessing effort [*Smith et al.*, 1996; *Reynolds and Marsico*, 1993]. Obviously, different users of the AVHRR data may wish to use different estimates of surface temperature when applying the NLSST algorithm. Users of local area coverage data in a region of little or no thermal gradients might apply a constant value of T_{SFC}. Alternatively, a regional user of AVHRR data who has no good a priori estimate of surface temperature might use the MCSST algorithm to define T_{SFC}. In this case, since gamma is made a function of the satellite measurements and because of the strong correlative effects described previously, a user should apply considerable effort to removing error sources in these measurements, such as residual cloud contamination.

4. Final Algorithm Adjustments and Comparison

Equations (5), (9), and (11) represent formal expressions of the MCSST, CPSST, and NLSST algorithms, the only difference between the algorithms being the functional form of Γ. In order to achieve the greatest possible accuracy, as determined from drifting buoy comparisons, and to include a correction for satellite viewing angle θ, as measured at Earth's surface, these equations are modified to

$$\mathrm{SST} = AT_4 + B\Gamma(T_4 - T_5) + C[\mathrm{Sec}\,(\theta) - 1](T_4 - T_5) + D \quad (12)$$

where the constant coefficients A, B, C, and D are determined by linear regression, using the drifting buoy measurements as ground truth, and are algorithm dependent. Equation (12) can be considered to be an empirical correction for and a generalization to the formal solutions for the split-window algorithms. The expression serves to correct or minimize certain error sources which may be present in the satellite measurements and are not properly handled by the formal solutions. Examples are faulty calibration of the AVHRR data, which can result in a temperature dependent bias error [*Walton et al.*, 1998], and global changes in the atmospheric content such as occur after a volcanic eruption. The satellite zenith angle term provides an empirical correction for off-nadir viewing angles. The multiplicative factor $(T_4 - T_5)$ has been found empirically to provide the greatest accuracy with the split-window equations. This term states that when $T_4 = T_5$, no zenith angle correction is needed, which suggests that, under this condition, there is little or no net atmospheric absorption of channel 4 and 5 radiance. If there were any net absorption, it should increase with increasing atmospheric pathlength. It is interesting to note that an expression identical to (12) applies to the multiple-channel algorithms using channel 3 (the dual and triple window algorithms), except that empirically it is found that a temperature difference multiplicative factor should not be included with the satellite zenith angle correction (see appendix). This implies that when $T_3 = T_4$, net radiation absorption exists in these channels (water vapor absorption in channel 4 and uniform mixed gas absorption in channel 3).

Table 2 provides a measure of the overall accuracy of the three algorithms both with simulation data and with NOAA 14 satellite measurements matched with drifting buoy measurements. The NOAA 14 NLSST, CPSST, and MCSST algorithms, which are computed separately with the simulation and the January 1996 open ocean data, are also provided in this table. The interesting result is that although the CPSST solution is the most accurate in simulation, the NLSST provides the least error when applied globally with satellite ocean temperature measurements. This result is a consequence of the impact of satellite measurement errors on the CPSST algorithm as described previously. The MCSST algorithm is not optimal with either data set.

To demonstrate the differences between the NLSST and MCSST algorithms with measured data, Figures 4 and 5 plot the effective gamma parameters, i.e., $B\Gamma$ (12), and the mean bias of these two algorithms, after modification, as a function of surface temperature and the AVHRR $T_4 - T_5$ channel difference, respectively. The mean bias values are computed from data placed in 4°C temperature bins (Figure 4) and 0.5°C temperature difference bins (Figure 5). These figures indicate that the NLSST algorithm, which is derived from the CPSST theoretical development, is more universal than is the MCSST in the sense that it introduces less bias at the extremes of the temperature and water vapor range. This result has been confirmed by a study performed at the Naval Research Laboratory (May 1993). In this study, NOAA 11 satellite SST retrieval matchups with drifting buoy measurements were obtained for the entire year of 1990. The satellite/buoy measurement comparisons were restricted to be within 2 hours and 10 km of each other, as suggested by *Minnett* [1990]. Half the data were used to derive coefficients for the MCSST, CPSST, and NLSST algorithms, and the other half were stratified to provide separate daytime and nighttime regional statistics. The daytime

Table 2. Daytime Split-Window Algorithm Comparison for Simulated Data and for NOAA 14 Open Ocean Satellite-Buoy Matchups

	Number of Matchups	Scatter, °C	Bias, °C
Simulation data			
MCSST	115	0.31	
CPSST	115	0.20	
NLSST	115	0.33	
January 1996 open ocean data			
MCSST	1967	0.60	
CPSST	1967	0.56	
NLSST	1967	0.52	
February 1996 open ocean data			
MCSST	1995	0.62	−0.01
CPSST	1995	0.57	0.00
NLSST	1995	0.53	0.01
March 1996 open ocean data			
MCSST	2085	0.66	−0.04
CPSST	2085	0.61	−0.02
NLSST	2085	0.57	0.00

	Simulation Equation
MCSST	$0.95876T_4 + 2.564(T_4 - T_5) - 261.68$
NLSST	$0.95168T_4 + 0.08655T_{sfc}(T_4 - T_5) - 259.09$
CPSST	$0.97847T_4 + \dfrac{0.12779T_4 - 34.175}{0.20136T_5 - 0.140238T_4 - 16.24} \cdot (T_4 - T_5) - 266.79$

	Open Ocean Equation (Daytime)
MCSST	$1.0222T_4 + 2.31(T_4 - T_5) - 280.39 + 0.83(T_4 - T_5) \cdot (\text{Sec}\ \theta - 1)$
NLSST	$0.9336T_4 + 0.079T_{sfc}(T_4 - T_5) - 253.69 + 0.77(T_4 - T_5) \cdot (\text{Sec}\ \theta - 1)$
CPSST	$0.9790T_4 + \dfrac{0.1414T_4 - 38.10}{0.214006T_5 - 0.171684T_4 - 10.14}(T_4 - T_5) - 266.84 + 0.86(T_4 - T_5)(\text{Sec}\ \theta - 1)$

See appendix for definitions of terms and symbols.

results are summarized in Figure 6. In every region, except the west Pacific, which has a scarcity of matchups, the NLSST(F), which applies the satellite temperature analysis described previously to define the gamma parameter, provides a significant reduction in RMSD error compared to the MCSST. The nighttime results summarized in Figure 7 are strikingly different. There appears to be no significant difference between the various algorithms. This null result is a consequence of the use of channel 3 (3.7 μm) in the nighttime algorithms. Simulation studies have demonstrated that radiation in this channel is only weakly absorbed by water vapor, the maximum attenuation in a moist atmosphere being approximately 2°C as compared to 9°C with channel 4 [*Weinreb and Hill*, 1980]. The approximations associated with the derivation of the MCSST algorithm, i.e., the constancy of the absorption coefficients, are apparently sufficient for SST algorithms using channel 3. The benefits obtained through the use of channel 3 are limited to nighttime measurements because reflected solar radiation can contaminate the emitted terrestrial signal during the day. By using channels 3, 4, and 5 at night in what is called a "triple window" equation, one minimizes the effect of instrumental noise in the algorithm. Examples of the various linear and nonlinear operational nighttime algorithms are provided by *May* [1993] and *Kidwell* [1995] and summarized in the appendix.

5. Discussion of 9-Year Time Series of Drifting Buoy Matchup Comparisons (1989–1997)

The previous sections have derived various linear and nonlinear SST algorithms from first principles and compared algorithm performance with common sets of test data. In this section, we provide a time series of the accuracy of the NOAA/NESDIS global operational SST product. Changes in accuracy over time reflect not only improvements in SST algorithms but also refinements in cloud detection and changes in the atmospheric state such as occur after a large volcanic eruption.

In order to measure the accuracy, monitor the quality, and detect errors in the NESDIS satellite-derived SST measurements, they are matched every day with temporally and spatially coincident drifting buoy measurements and placed in an "SST match file." The buoy data set used for matching with the satellite SST measurements is the global set of drifting buoys which broadcast data to the French-built Data Collection System (DCS) carried on board the NOAA POES series of satellites. These data are (1) received by NESDIS, (2) processed and Earth-located by Service Argos in the United States, (3) quality checked by the NOAA National Weather Service, and (4) placed in 6-hour synoptic marine observation files of the National Centers for Environmental Prediction (formerly the National Meteorological Center) for use as input to the global meteorological and ocean models. NESDIS retrieves buoy data from these files and stores them in a file containing buoy data for the past month.

Once per day, matches are attempted between all the satellite and buoy observations obtained in the previous 24 hours. For each satellite observation, a record is added to the SST match file if there is a matching buoy observation within 100 km and 24 hours. This record contains (1) all the pertinent satellite observation data, such as time, location, SST, satellite and solar angles, and individual AVHRR channel temperatures or reflectances, (2) all the pertinent buoy data such as SST, time, and location, (3) the time and location difference between the satellite and buoy measurement, and (4) information such as SST and gradient from the latest NESDIS global satellite SST 100 km analyzed field. At the end of each month, all matches within 4 hours and 25 km are extracted from the SST Match File. Before the monthly global statistics are generated, a final quality control procedure is applied to the matchups. First, in order to remove the infrequent faulty buoy reports (i.e., reports with incorrect location or with transmission errors), the buoy temperatures are constrained to agree to within 3°C of either a climatological or a satellite-derived temperature analysis of SST. Second, in order to provide a stable set of monthly global statistics, no buoy and satellite measurements which differ from each other by more than 4°C are included in the statistics. This requirement primarily removes matchups in high thermal gradient regions such as the Gulf Stream, and typically no more than one or two such matchups are removed with this test each month.

The number of matches obtained with the above procedure has grown from about 500 for both day and night during the years 1989–1992 to over 2000 during 1996 and 1997 (see Figure 8). The quality-controlled matches are used to calculate day and night monthly mean satellite-buoy SST difference (i.e., bias) and standard deviation of the satellite-buoy SST differ-

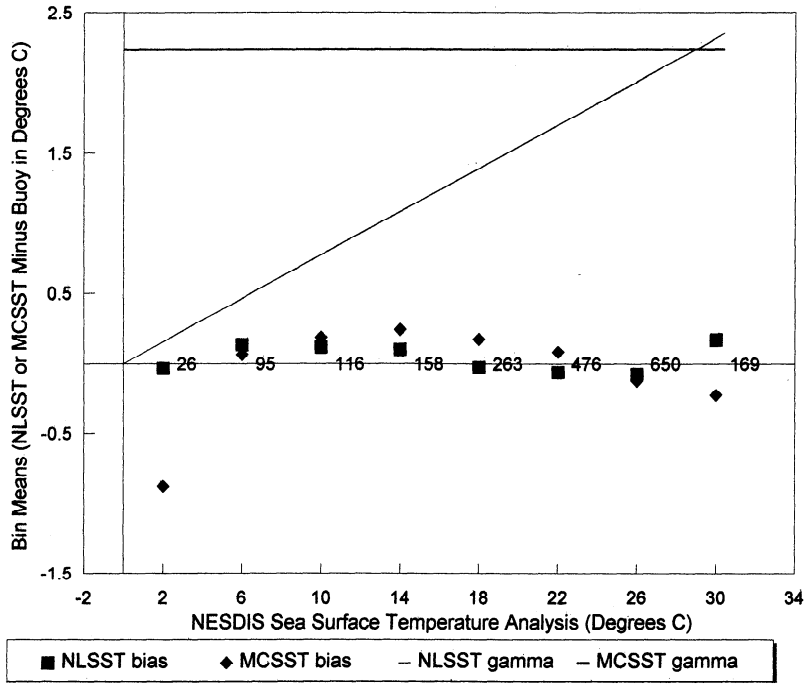

Figure 4. The mean gamma parameter values and bias (in degrees Celsius) of the NLSST and MCSST algorithms for all satellite data falling within 4°C temperature bins of the NESDIS 100 km SST analysis. The data legends indicate the number of January 1996 satellite-buoy matchups included in each bin. The symbols are positioned at the center of each bin.

ences (i.e., scatter). Figures 9 and 10 show the monthly bias and scatter time series for the period 1989–1997 for day and night, respectively. On the bottom portion of Figures 9 and 10 are three timelines. The first timeline gives the periods when different satellites were used. The second shows when the form of the SST equations were changed. The third timeline indicates when SST equations were updated. See Tables 3–5 for a listing of the operational SST equations used since 1989. De-

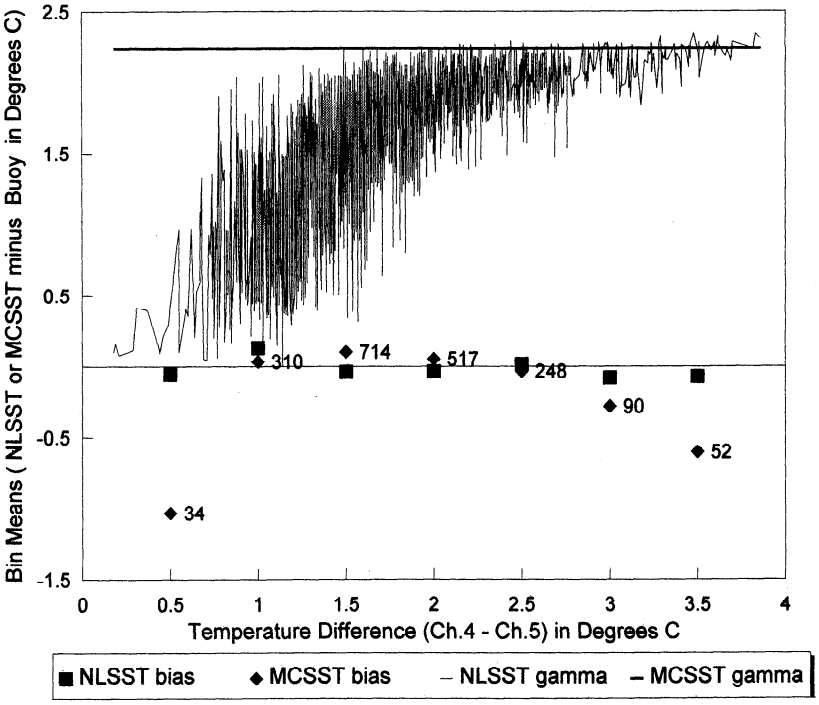

Figure 5. The mean gamma parameter values and bias (in degrees Celsius) of the NLSST and MCSST algorithms for all satellite data falling within 0.5°C temperature difference bins of AVHRR channel 4 − channel 5 measurements. The data legends indicate the number of January 1996 satellite-buoy matchups included in each bin. The symbols are positioned at the center of each bin.

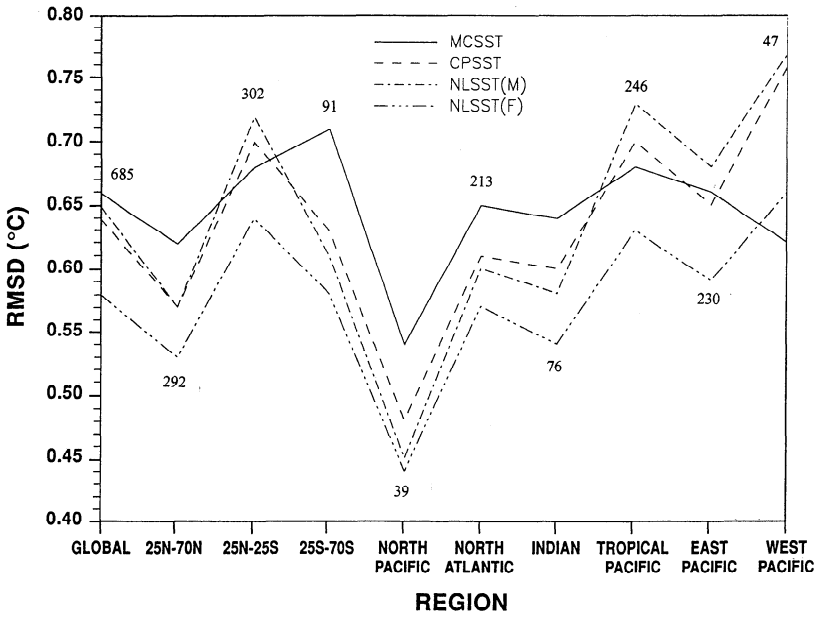

Figure 6. RMS regional errors of the daytime split-window MCSST, CPSST, and NLSST algorithms. Two NLSST algorithms are included: the NLSST(M) uses the MCSST temperature measurement as the surface temperature estimate, while the NLSST(F) uses the 100 km satellite surface temperature analysis for T_{sfc}. The data legends indicate the number of satellite-buoy matchups in each region.

tails of changes in algorithms, satellites, and cloud tests can be found in the work by *Kidwell* [1995]. The National Climatic Data Center maintains an on-line version of this document at http://www2.ncdc.noaa.gov/POD/intro.htm.

Figure 9 shows a 9-year time series of the satellite-buoy matchup statistics for the years 1989–1997 for daytime matches. The upper graph depicts the scatter of the temperature differences (satellite SST minus buoy SST), while the lower graph depicts the bias. The daytime scatter has declined over the years from about 0.8°C to values approaching 0.5°C. The bias has stayed between −0.2°C and +0.4°C, with one exception, which corresponds with the eruption of Mount Pinatubo in June 1991 [*Reynolds*, 1993]. The sulfuric acid aerosols created in the stratosphere from this volcanic eruption attenuated infrared radiation causing negative biases (i.e., lower satellite SST measurements) initially in the tropics and eventually into midlatitudes. On a global average basis, daytime satellite SST measurements were over 0.5°C low, with

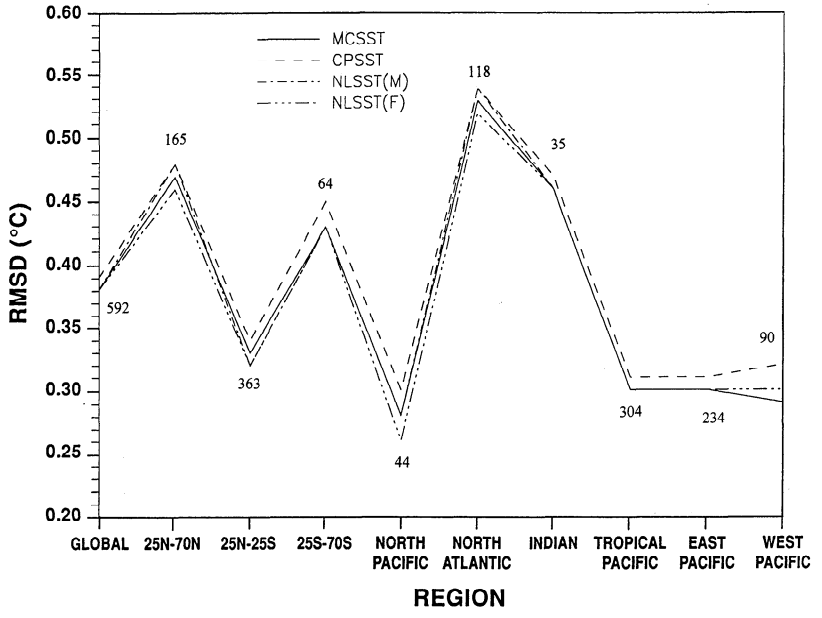

Figure 7. RMS regional errors of the nighttime triple-window MCSST, CPSST, and NLSST algorithms. Two NLSST algorithms are included: the NLSST(M) uses the MCSST temperature measurement as the surface temperature estimate, while the NLSST(F) uses the 100 km satellite surface temperature analysis for T_{sfc}. The data legends indicate the number of satellite-buoy matchups in each region.

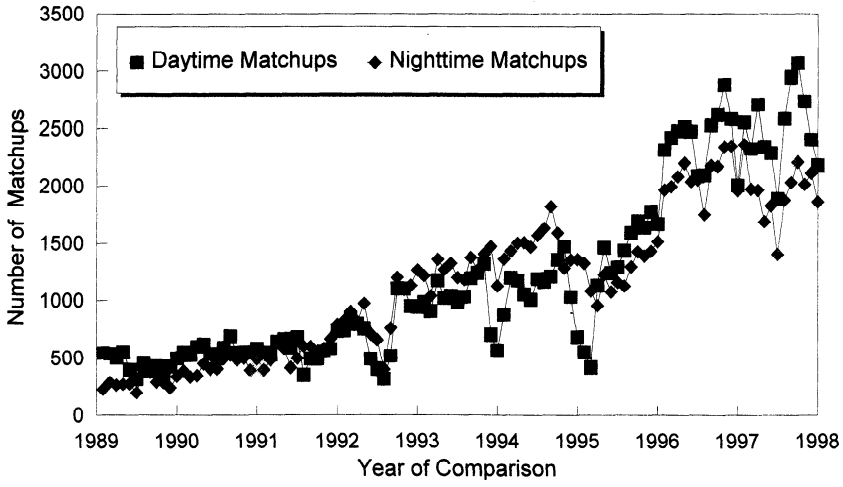

Figure 8. Nine-year time series of satellite-buoy matchup statistics: number of daytime and nighttime matchups per month.

biases in tropical latitudes exceeding −2.0°C. The bias improved to about −0.25°C after the equation update on April 9, 1992, and then gradually increased as the aerosols dissipated, returning to normal levels after the equation update on June 14, 1993. Thus the effects of Mount Pinatubo lasted for 2 years, from June 15, 1991 to June 14, 1993. It should be noted that the daytime scatter improved significantly, however, using the NLSST algorithm after the effects of Mount Pinatubo had dissipated. This improvement agrees with the improvement associated with the NLSST algorithm demonstrated in Figure 6. One could infer that some of this improvement might be attributed to the increasing number of matchups during the same period. However, this is not likely, since no equivalent reduction in the nighttime scatter has been observed (see Figure 10).

For nighttime matches (Figure 10) the Mount Pinatubo eruption also caused the greatest accuracy anomaly in the buoy time series. The global average bias reached a low of just under −0.5°C, with a maximum scatter of 0.9°C. On October 3, 1991, in response to the Mount Pinatubo eruption, an alternative nighttime algorithm (a different form of the linear MCSST triple-window equation called the "volcano SST equation") was implemented which has been demonstrated to be relatively insensitive to volcanic aerosols, while still providing an accurate correction for atmospheric water vapor absorption [*Wal-*

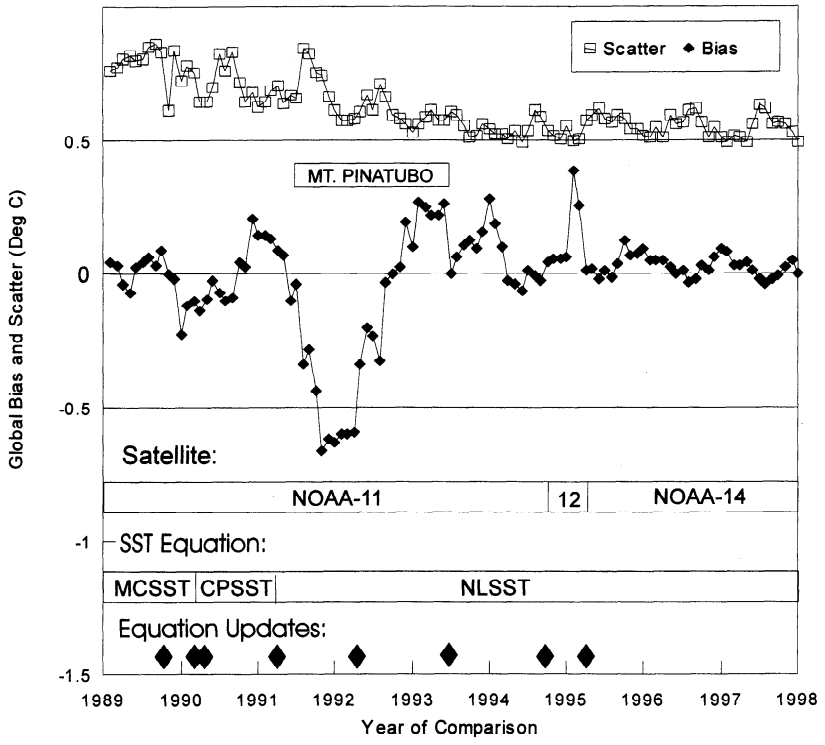

Figure 9. Nine-year time series of satellite-buoy matchup statistics: daytime global monthly bias (i.e., mean satellite-buoy SST difference) and scatter (i.e., standard deviation of satellite-buoy SST difference). The timelines at the bottom of the figure indicate when satellite and SST equation changes were made.

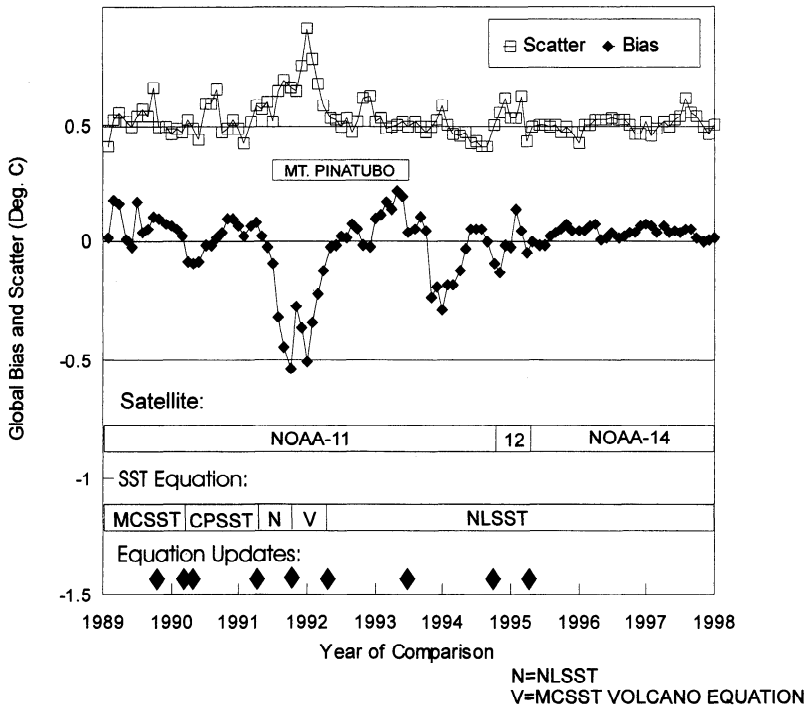

Figure 10. Nine-year time series of satellite-buoy matchup statistics: nighttime global monthly bias (i.e., mean satellite-buoy SST difference) and scatter (i.e., standard deviation of satellite-buoy SST difference). The timelines at the bottom of the figure indicate when satellite and SST equation changes were made.

ton, 1985]. Unfortunately, this alternative algorithm is very sensitive to instrumental noise and to a nighttime channel 3 calibration error which is associated with direct sunlight impinging upon the AVHRR instrument as the Sun rises above the limb of Earth [*Walton et al.*, 1998]. It was not until a standard nighttime NLSST equation was reinstated on April 9, 1992, that the satellite SST accuracy returned to near-normal levels. During the remainder of 1992, the volcanic aerosols dissipated, and a positive bias in the nighttime satellite SST measurements increased until the NLSST equation was updated again on June 11, 1993. The other large negative bias period at the end of 1993 may be related to the channel 3 calibration error associated with the sunlight problem discussed above. Except for the Mount Pinatubo period, nighttime scatter has generally been very consistent at about 0.5°C. Unlike the case in the daytime, nighttime algorithm changes have had little impact on accuracy, a result which is also demonstrated with Figure 7.

In summary, since NOAA 14 became the operational satellite for SST in March 1995, the accuracy of the NLSST measurements has been very consistent and sufficient for many,but not all, of the applications discussed in the introduction to this paper. The improvement in the daytime scatter from 0.8 to 0.5°C between 1989 and the end of 1997 is due partly to improved SST algorithms and partly to improvements in the cloud detection procedures.

6. Conclusion

This paper describes certain improvements in the production of SST from AVHRR data which have recently been applied in the global production of SST at NESDIS and at the

Table 3. NESDIS Daytime Operational SST Equations

Date	Satellite	Type	SST Equation
Sept. 27, 1989	NOAA 11	MCSST split	$1.01345T_4 + 2.659762(T_4 - T_5) + 0.526548(T_4 - T_5)(\text{Sec}\,\theta - 1) - 277.742$
March 2, 1990	NOAA 11	CPSST split	$0.94575T_5 + \dfrac{0.19410T_5 - 48.15}{0.20524T_5 - 0.17334T_4 - 6.25}(T_4 - T_5 + 1.32) + 0.60(T_4 - T_5)(\text{Sec}\,\theta - 1) - 261.0$
April 18, 1990	NOAA 11	CPSST split	$0.92912T_5 + \dfrac{0.19069T_5 - 49.16}{0.20524T_5 - 0.17334T_4 - 6.78}(T_4 - T_5 + 0.789) + 0.81(T_4 - T_5)(\text{Sec}\,\theta - 1) - 254.18$
April 10, 1991	NOAA 11	NLSST split	$0.94649T_4 + 0.08412T_{\text{sfc}}(T_4 - T_5) + 0.751(T_4 - T_5)(\text{Sec}\,\theta - 1) - 257.20$
April 9, 1992	NOAA 11	NLSST split	$0.962191T_4 + 0.083398T_{\text{sfc}}(T_4 - T_5) + 0.65375(T_4 - T_5)(\text{Sec}\,\theta - 1) - 261.114$
June 14, 1993	NOAA 11	NLSST split	$0.92323T_4 + 0.082523T_{\text{sfc}}(T_4 - T_5) + 0.463038(T_4 - T_5)(\text{Sec}\,\theta - 1) - 250.109$
Sept. 15, 1994	NOAA 12	NLSST split	$0.876992T_4 + 0.083132T_{\text{sfc}}(T_4 - T_5) + 0.349877(T_4 - T_5)(\text{Sec}\,\theta - 1) - 236.667$
March 20, 1995	NOAA 14	NLSST split	$0.939813T_4 + 0.076066T_{\text{sfc}}(T_4 - T_5) + 0.801458(T_4 - T_5)(\text{Sec}\,\theta - 1) - 255.165$

Table 4. NESDIS Nighttime Operational SST Equations

Date	Satellite	Type	SST Equation
Sept. 27, 1989	NOAA 11	MCSST triple	$1.036027T_4 + 0.892857(T_3 - T_5) + 0.520056(T_3 - T_5)(\text{Sec}\ \theta - 1) - 282.373967$
March 2, 1990	NOAA 11	CPSST triple	$0.97778T_4 + \frac{0.16949T_4 - 54.11}{0.20524T_5 - 0.07747T_3 - 41.60}(T_3 - T_5 - 6.73) + 1.41(\text{Sec}\ \theta - 1) - 258.99$
April 18, 1990	NOAA 11	CPSST triple	$0.97120T_4 + \frac{0.16835T_4 - 34.32}{0.20524T_5 - 0.07747T_3 - 20.01}(T_3 - T_5 + 14.86) + 1.87(\text{Sec}\ \theta - 1) - 276.59$
April 10, 1991	NOAA 11	NLSST triple	$1.0006T_4 + 0.245(T_3 - T_5) + 0.02766T_{sfc}(T_3 - T_5) + 1.88(\text{Sec}\ \theta - 1) - 272.36$
Oct. 3, 1991	NOAA 11	MCSST triple	$1.011015T_5 + 2.088810(T_3 - T_4) + 2.278617(\text{Sec}\ \theta - 1) - 273.234$
April 9, 1992	NOAA 11	NLSST dual	$1.032274T_4 + 0.055297T_{sfc}(T_3 - T_4) + 2.125323(\text{Sec}\ \theta - 1) - 280.212$
June 11, 1993	NOAA 11	NLSST triple	$0.970625T_4 + 0.035216T_{sfc}(T_3 - T_5) + 1.522429(\text{Sec}\ \theta - 1) - 263.231$
Sept. 15, 1994	NOAA 12	NLSST triple	$0.963368T_4 + 0.033139T_{sfc}(T_3 - T_5) + 1.731971(\text{Sec}\ \theta - 1) - 260.854$
March 20, 1995	NOAA 14	NLSST triple	$0.980064T_4 + 0.031889T_{sfc}(T_3 - T_5) + 1.817861(\text{Sec}\ \theta - 1) - 266.186$

Naval Oceanographic Office. Nonlinear SST algorithms have been developed which provide a lower scatter of the split-window satellite estimates of SST against buoy measurements than does the linear MCSST algorithm. This result has been demonstrated both with simulation data and with real open ocean AVHRR data, although the optimal functional form of the nonlinear algorithm, i.e., its dependence upon the channel 4 − 5 temperature difference, is quite different with these two data sets. This result suggests that there may not be a single "optimal algorithm" for all user applications or all data sets.

A similar result was reported in a recent paper by *Barton* [1995], in which he compares various SST algorithms which have been developed for use with AVHRR data. He finds that all the algorithms can be compared in terms of a constant effective gamma parameter, i.e., $B\Gamma$ of (12). In a tropical atmosphere the various algorithms have gamma values which range from 1.5 to 3. Barton suggests that this variation results from a differing noise content within the AVHRR data sets from which these algorithms are developed. The noise content or data quality of an AVHRR/buoy matchup data set is perhaps most sensitive to any residual cloud contamination of the measured data as well as instrumental noise. Other factors which can affect data quality include large differences between the ocean's skin temperature and the underlying mixed layer or bulk ocean temperature as well as the presence of any tropospheric or stratospheric aerosols within the field-of-view of the AVHRR measurements. We have demonstrated here that not only the magnitude of the gamma parameter is affected by the quality of the data but also its functional dependence upon temperature and/or the channel temperature difference.

Appendix

Tables 3 and 4 list the daytime and nighttime, respectively, operational SST equations that have been used in NESDIS since 1989. For the most part, they represent a progression from linear MCSST equations to nonlinear CPSST and NLSST equations. Usually, split-window (i.e., channels 4 and 5) equations are used for daytime SST, and triple window (i.e., using channels 3, 4, and 5) equations are used at night. An exception to this rule occurred from October 3, 1991 to June 10, 1993, when first a nighttime MCSST triple window and then a nighttime NLSST dual window (i.e., channels 3 and 4) equation was used to compensate for the effects of stratospheric aerosols from the Mount Pinatubo volcanic eruptions.

The following terms appear in these equations.

SST sea surface temperature in degrees Celsius;

T_3, T_4, T_5 equivalent blackbody temperature in Kelvins for AVHRR channels 3 (3.7 μm), 4 (11.0 μm), and 5 (12.0 μm); the nonlinearity AVHRR calibration corrections for channels 4 and 5 should be applied to the AVHRR temperatures before using the equations in these tables [see *Kidwell*, 1995];

T_{sfc} an a priori estimate of the SST derived from the closest NESDIS global analyzed SST field value (1° latitude/longitude grid) in degrees Celsius; T_{sfc} is restricted to the range −2°–28°C; it is possible to use other sources for T_{sfc}, such as a climatological SST or even a satellite-derived SST estimated with a linear MCSST equation;

Sec θ secant of the satellite zenith angle.

As a result of the Shared Processing Program agreements approved between the Department of the Navy, the Department of the Air Force, and NOAA regarding the sharing of satellite data, the Naval Oceanographic Office (NAVOCEANO) has been operationally producing SST retrievals since the launch of NOAA 14 on an orbit-by-orbit basis, using procedures similar to those described by *McClain et al.* [1985]. In addition to incorporating all of the recent SST product improvements described in this paper, NAVOCEANO has also incorporated additional modifications important to them, such as increasing the density of coastal retrievals worldwide and extending SST retrieval capability from 70°N to 80°N latitude. The NAVOCEANO NLSST generation process, algorithm coefficients, and buoy matchup statistics are described by *May et al.* [1998]. Table 5 lists the coefficients used by NAVOCEANO for NOAA 14.

Table 5. Naval Oceanographic Office Operational SST Equations

Date	Satellite	Type	SST Equation
March 20, 1995	NOAA 14	NLSST split day	$0.9355T_4 + 0.0780T_{sfc}(T_4 - T_5) + 0.8009(T_4 - T_5)(\text{Sec}\ \theta - 1) - 254.0163$
March 20, 1995		NLSST triple night	$0.9796T_4 + 0.032T_{sfc}(T_3 - T_5) + 1.8106(\text{Sec}\ \theta - 1) - 266.1146$

Acknowledgment. The authors wish to thank Ian Barton, Guillermo Podesta, and Peter Cornillon for their valuable comments and suggestions during the review of this paper.

References

Barton, I. J., Satellite-derived sea surface temperatures: Current status, *J. Geophys. Res.*, *100*, 8777–8790, 1995.

Barton, I. J., A. M. Zavody, D. M. O'Brien, D. R. Cutten, R. W. Saunders, and D. T. Llewellyn-Jones, Theoretical algorithms for satellite-derived sea surface temperatures, *J. Geophys. Res.*, *94*, 3365–3375, 1989.

Bates, J. J., and H. F. Diaz, Evaluation of multi-channel sea surface temperature product quality for climate monitoring, *J. Geophys. Res.*, *96*, 20,613–20,622, 1991.

Breaker, L., V. Krasnopolsky, D. B. Rao, and X.-H. Yan, The feasibility of estimating ocean surface currents on an operational basis using satellite feature tracking methods, *Bull. Meteorol. Soc.*, *75*(11), 2085–2095, 1994.

Chester, A., and N. Wolfe, NOAA's CoastWatch for the Southeast—Viewpoint from the field, in *Proceedings of the '90 Conference, September, 26–28, 1990*, Mar. Technol. Soc., Washington, D. C., pp. 561–565, 1990.

Cornillon, P. (Chair), *Sea Surface Temperature Products for the Oceanographic Scientific Research Community: A Report of the Sea Surface Temperature Archiving Science Working Group*, 36 pp., NASA and NOAA, Joint Oceanogr. Inst., Inc., Washington, D. C., 1989.

Emery, W. J., Y. Yu, G. A. Wick, P. Schluessel, and R. W. Reynolds, Correcting infrared satellite estimates of sea surface temperature for atmospheric water vapor attenuation, *J. Geophys. Res.*, *99*, 5219–5236, 1994.

Epperly, S., J. Braun, A. Chester, F. Cross, J. Merriner, and P. Tester, Winter distribution of sea turtles in the vicinity of Cape Hatteras and their interactions with the summer flounder trawl fishery, *Bull. Mar. Sci.*, *56*(2), 547–568, 1995.

Hagan, D. E., A basic limitation of the split window method for SST retrievals when applied to a wide range of water vapor conditions, *Geophys. Res. Lett.*, *16*(8), 815–817, 1989.

Harris, A. R., and I. M. Mason, An extension to the split-window technique giving improved atmospheric correction and total water vapor, *Int. J. Remote Sens.*, *13*, 881–892, 1992.

Hussey, J. (Ed.), *ENVIROSAT—2000 Report NOAA Satellite Requirements Forecast*, 121 pp., NOAA, Washington, D. C., 1985.

Jacobowitz, H. (Ed.), *Climate Measurement Requirements for the National Polar-orbiting Operational Environmental Satellite System (NPOESS) Workshop Report*, 71 pp., Univ. Corp. for Atmos. Res., Boulder, Colo., 1997.

Ji, M., A. Leetma, and J. Derber, An ocean analysis system for seasonal to interannual climate studies, *Mon. Weather Rev.*, *123*(2), 460–481, 1995.

Kidwell, K., *NOAA Polar Orbiter Data Users Guide*, 412 pp., NOAA/NESDIS/NCDC, Washington, D. C., 1995.

Laurs, R., and J. Brucks, Living marine resources applications, in *Satellite Oceanic Remote Sensing*, edited by B. Saltzman, *Adv. Geophys.*, *27*, 419–452, 1985.

May, D. A., Global and regional comparative performance of linear and nonlinear satellite multichannel sea surface temperature algorithms, *Rep. NRL/MR/7240-93-7049*, 34 pp., Nav. Res. Lab., Washington, D. C., 1993.

May, D. A., M. M. Parmeter, D. S. Olszewski, and B. D. McKenzie, Operational processing of satellite sea surface temperature retrievals at the Naval Oceanographic Office, *Bull. Am. Meteorol. Soc.*, *79*(3), 397–407, 1998.

McClain, E. P., W. G. Pichel, and C. C. Walton, Comparative performance of AVHRR-based multichannel sea surface temperatures, *J. Geophys. Res.*, *90*, 11,587–11,601, 1985.

McMillin, L. M., Estimation of sea surface temperatures from two infrared window measurements with different absorption, *J. Geophys. Res.*, *80*, 5113–5117, 1975.

McMillin, L. M., and D. S. Crosby, Theory and validation of the multiple window sea surface temperature technique, *J. Geophys. Res.*, *89*, 3655–3661, 1984.

Minnett, P., The regional optimization of infrared measurements of sea surface temperature from space, *J. Geophys. Res.*, *95*, 13,497–13,510, 1990.

Myers, D., and P. Hick, An application of satellite-derived sea surface temperature data to the Australian fishing industry in near real-time, *Int. J. Remote Sens.*, *11*(11), 2103–2112, 1990.

Prabhakara, C., G. Dalu, and V. G. Kunde, Estimation of sea surface temperature from remote sensing in the 11- to 13-μm window region, *J. Geophys. Res.*, *79*, 5039–5044, 1974.

Prabhakara, C., R. S. Fraser, G. Dalu, M. C. Wu, and R. J. Curran, Thin cirrus clouds: Seasonal distribution over oceans deduced from Nimbus 4 IRIS, *J. Appl. Meteorol.*, *27*, 379–399, 1988.

Reynolds, R. W., Impact of Mount Pinatubo aerosols on satellite-derived sea surface temperatures, *J. Clim.*, *6*(4), 768–774, 1993.

Reynolds, R., and E. Marsico, An improved real-time global sea surface temperature analysis, *J. Clim.*, *6*, 114–119, 1993.

Reynolds, R., C. Folland, and D. Parker, Biases in satellite-derived sea-surface-temperature data, *Nature*, *341*(6244), 728–731, 1989.

Robinson, M. K., Atlas of North Pacific Ocean monthly mean temperatures and mean salinities of the surface layer, *Rep. N00 RP-2*, 194 pp., Nav. Oceanogr. Off., Washington, D. C., 1976.

Sakaida, F., and H. Kawamura, Estimation of sea surface temperatures around Japan using the advanced very high resolution radiometer (AVHRR)/NOAA-11, *J. Oceanogr.*, *48*, 179–192, 1992.

Schwab, D., and K. Bedford, Initial implementation of the Great Lakes Forcasting System: A real-time system for predicting lake circulation and thermal structure, *Water Pollut. Res. J. Can.*, *29*(2–3), 203–220, 1994.

Sherman, J., R. Edwards, and J. Apel (Chairs), Workshop support documentation, vol. II, in *NOAA Workshop on Oceanic Remote Sensing, Estes Park, Colorado, August 19–24, 1979*, 136 pp., Natl. Oceanic and Atmos, Admin., Washington, D. C., 1980.

Simpson, J. J., Remote sensing in fisheries: A tool for better management in the utilization of a renewable resource, *Can. J. Fish. Aquat. Sci.*, *51*, 743–771, 1994.

Smith, E., J. Vazquez, A. Tran, and R. Sumagaysay, Satellite-derived sea surface temperature data available from the NOAA/NASA pathfinder program, *Eos Trans. AGU Electron. Suppl.*, 1996. (Available at http://www. agu.org/eos_elec/95274e.html)

Smith, W. L., H. M. Woolf, P. G. Abel, C. M. Hayden, M. Chalfant, and N. Grody, NIMBUS-5 sounder data processing system, *NOAA Tech. Memo., NESS 57*, 99 pp., 1974.

Sobrino, J. A., Z. L. Li, and M. P. Stoll, Impact of the atmospheric transmittance and total water vapor content in the algorithms for estimating satellite sea surface temperatures, *IEEE Trans. Geosci. Remote Sens.*, *31*, 946–952, 1994.

Strong, A., Monitoring El Niño using satellite based sea surface temperature, *Ocean Air Interactions*, *1*, 11–28, 1986.

Strong, A. E., C. S. Barrientos, C. Duda, and J. Sapper, Improved techniques for monitoring coral reef bleaching, *Proc. 8th Int. Coral Reef Symp.*, *2*, 1495–1498, 1997.

Walton, C. C., Satellite measurement of sea surface temperature in the presence of volcanic aerosols, *J. Clim. Appl. Meteorol.*, *24*, 501–507, 1985.

Walton, C. C., The AVHRR/HIRS operational method for satellite based sea surface temperature determination, *NOAA Tech. Rep., NESDIS 28*, 58 pp., 1987.

Walton, C. C., Nonlinear multichannel algorithms for estimating sea surface temperature with AVHRR satellite data, *J. Appl. Meteorol.*, *27*, 115–124, 1988.

Walton, C. C., J. T. Sullivan, C. R. Nagaraja Rao, and M. P. Weinreb, Corrections for detector nonlinearities and calibration inconsistencies of the infrared channels of the advanced very high resolution radiometer, *J. Geophys. Res.*, *103*, 3323–3337, 1998.

Weinreb, M. P., and M. L. Hill, Calculation of atmospheric radiances and brightness temperatures in infrared window channels of satellite radiometers, *NOAA Tech. Rep., NESS 80*, 49 pp., 1980.

Yates, H., D. Cotter, and G. Ohring, *ENVIROSAT-2000 Report, Operational Satellite Support to Scientific Programs*, 50 pp., NOAA, Washington, D. C., 1985.

Yokoyama, R., and S. Tanba, Estimation of sea surface temperature via AVHRR of NOAA-9—Comparison with fixed buoy data, *Int. J. Remote Sens.*, *12*, 2513–2528, 1991.

Yu, Y., and I. J. Barton, A non-regression-coefficients method of sea surface temperature retrieval from space, *Int. J. Remote Sens.*, *15*, 1189–1206, 1994.

D. A. May, Naval Oceanographic Office, Code N212, Department the Navy, Building 1002, Stennis Space Center, Mississippi 39529.

W. G. Pichel, J. F. Sapper, and C. C. Walton, NOAA, National Environmental Satellite, Data, and Information Service, NSC Room 102, Stop 9910, 4700 Silver Hill Road, Washington, D. C. 20233-9910. (e-mail: wpichel@nesdis.noaa.gov)

(Received October 23, 1996; revised June 15, 1998; accepted July 15, 1998.)